Hybrid Nanomaterials

Deutsche Ausgabe: DOI: 10.1002/ange.201505319
Internationale Ausgabe: DOI: 10.1002/anie.201505319

Chiral Carbonaceous Nanotubes Modified with Titania Nanocrystals: Plasmon-Free and Recyclable SERS Sensitivity**

Bocheng Qiu, Mingyang Xing, Qiuying Yi, and Jinlong Zhang**

Abstract: *Chiral carbonaceous nanotubes (CNT) were successfully used in plasmon-free surface-enhanced Raman scattering (SERS) for the first time. Further modification of TiO_2 nanocrystals on the chiral CNTs successfully realized the recycling of SERS substrate as chiral CNT/TiO_2 hybrids. The high SERS sensitivity of methylene blue (MB) over the chiral CNT/TiO_2 hybrids is ascribed to the laser-driven birefringence induced by the helical structure, which provides much more opportunities for the occurrence of Raman scattering. The TiO_2 nanocrystals highly dispersed on the surface and inside the hollow cavity of chiral CNTs can completely degrade the MB under the solar light irradiation, leading to the self-cleaning of SERS substrate. The present research opens a new way for the application of chiral inorganic materials in plasmon-free SERS detection.*

Since ordered chiral mesoporous SiO_2 was synthesized by a surfactant-template method in 2004,[1] some other chiral inorganic materials, such as carbonaceous nanotubes,[2] g-C_3N_4,[3] TiO_2,[4] and other metal oxide complexes,[5] were also prepared by using the similar template technology. Although the chiral inorganic materials have attracted much attention in recent years owing to their optimized morphology and texture as well as unique chirality and optical activity, the variety of practical applications has always been restricted; they have almost always focused on the catalysis,[6] chemical and biological sensors,[7] and optical devices.[8] Actually, some chiral inorganic materials with excellent electroconductivity, optical activity, and thermal stability is an ideal support, which can greatly extend its application range, for instance, the new development of chiral carbon-based nanotubes in the application of surface-enhanced Raman scattering (SERS).

As a fast and sensitive means for nondestructive detection of molecules and ions, SERS has aroused much interest in analysis, chemistry, and biology fields.[9] However, most of reported materials used in the SERS require the loading of noble metals such as Au, Ag, and Cu, which has largely limited the practical applications owing to their high cost, low stability, poor biocompatibility, and lack of reusability.[10] Hence, the development of noble-metal-free materials employed in the SERS detection with the improved and recyclable SERS sensitivity is very necessary. Recently, some plasmonic-enhancer-free materials with self-cleaning properties were employed in the SERS detection. For instance, Alessandri found that the TiO_2 shell-based spherical resonators in the absence of plasmonic enhancers also could lead to a remarkable enhancement of Raman scattering by the synergistic combination of high refractive index of the shell layer, multiple light scattering through the spheres, and related geometrical factors.[11] Moreover, the TiO_2 offered a self-cleaning platform owing to its excellent photocatalytic activity. Our previous work also adopted a plasmon-free TiO_2 photonic microarray to achieve the improvement of SERS sensitivity by the light-matter coupling,[9] which also could be quickly recovered under simulated solar light irradiation and repeatedly used. As an ideal photocatalyst, TiO_2 has been widely used in self-cleaning development. Alessandri and co-workers have carried out much research work on the TiO_2-based functional materials with self-cleaning properties. They used the plasmonic heating of gold nanoparticles to generate local SERS-active TiO_2 spots, which could photodegrade the detected methylene blue (MB) molecules under the UV light irradiation.[12] Additionally, they reported another Au/TiO_2 micrometric spots on polymeric colloidal crystals to enhance the SERS sensitivity.[13] This blend is photoactive and also can be conveniently modified or completely removed by the laser irradiation.

Herein, we used the C_{18}-L/D-Glu enantiomers as the template and pyrrole as the carbon precursors to synthesize the chiral polypyrrole nanotubes, and transformed into carbonaceous nanotubes (CNT) by the carbonization process, then employed a one-step solvothermal method to load the highly dispersed TiO_2 nanocrystals on the CNT to prepare the R-CNT/TiO_2 (right-handed lipid) and L-CNT/TiO_2 (left handed lipid), respectively. All of the prepared chiral CNTs exhibited plasmon-free and recyclable SERS sensitivity. Their chiral helical structure will induce the birefringence and generate the Kerr effect under the irradiation of laser at the macroscopic scale, which is beneficial to the improvement of SERS sensitivity of the MB. Simultaneously, the loading of

[*] Dr. B. C. Qiu, Dr. M. Y. Xing, Q. Y. Yi, Prof. Dr. J. L. Zhang
Key Laboratory for Advanced Materials and Institute of Fine Chemicals, East China University of Science and Technology
130 Meilong Road, Shanghai 200237 (P.R. China)
E-mail: mingyangxing@ecust.edu.cn
jlzhang@ecust.edu.cn
Prof. Dr. J. L. Zhang
Department of Chemistry, Tsinghua University
Beijing 100084 (P.R. China)

[**] This work has been supported by National Nature Science Foundation of China (21203062, 21377038, 21173077, 21237003), the National Basic Research Program of China (973 Program, 2013CB632403), the Research Fund for the Doctoral Program of Higher Education (20120074130001), the Fundamental Research Funds for the Central Universities (22A201514021), and sponsored by "Chenguang Program" supported by Shanghai Education Development Foundation and Shanghai Municipal Education Commission (14CG30).

Supporting information for this article is available on the WWW under http://dx.doi.org/10.1002/anie.201505319.

TiO_2 leads to the photodegradation of MB, which is responsible for the recyclable nature of chiral CNTs.

For the preparation, the chiral polypyrrole (PPy) nanotubes were templated by self-assembly of enantiopure chiral C_{18}-L/D-Glu molecules and subsequent polymerization of the bound pyrroles.[2,14] Then, the enantiopure chiral R/L-CNTs were prepared by the carbonization of self-assembled chiral PPy nanotubes.[2] All of the prepared chiral PPy and CNT have the helical structures and mirror-imaged circular dichroism (CD) signals. For instance, the right-handed lipids of R-PPy and R-CNT all show a smooth surface and obvious ordered helical arrangement of the polymers or carbon nanostructures, as shown in SEM images (Supporting Information, Figure S1 a–d). TEM images give a remarkable hollow structure (pipe diameter size of ca. 30 nm) of nanotubes (Supporting Information, Figure S1 e–h), which is beneficial to the loading of TiO_2 nanocrystals highly dispersed inside the tubes. Just like the R-PPy and R-CNT, the prepared L-PPy and L-CNT also present smooth surface and ordered helical structure, as well as the hollow inner cavity (Supporting Information, Figure S2). Additionally, the ordered helical structures determines the obvious mirror-imaged CD signals on the chiral materials (Supporting Information, Figure S3), indicating that the helical structure rotates the incident light in a different direction, clockwise or counter-clockwise, giving rise to induced birefringence at the microscopic scale,[15] which is expected to improve the SERS sensitivity.

To demonstrate the carbonization of CNT, the FTIR spectra of R-PPy nanotubes before and after heating under a flow of N_2 are shown in the Supporting Information, Figure S4. After the carbonization, the characteristic peaks of pyrrole rings at 1549 and 1470 cm^{-1} and the bands characteristic for stretching of conjugated C–N and planar C–H at 1302 and 1040 cm^{-1} all decrease obviously compared to the R-PPy nanotubes without heating treatment, indicating the transformation from R-PPy to R-CNT.

As an ideal photocatalyst, TiO_2 has many advantages, such as low toxicity, low-cost, and superior photocatalytic performance,[16] and it is chosen as a cleaner for in situ growth on the chiral CNTs in the present work (the percentage of TiO_2 is approximate 17.5 wt%, as shown in the TGA result in the Supporting Information, Figure S5). The FESEM images are given in Figure 1 to show the micromorphology of R-CNT/TiO_2. It is obvious that the chiral CNTs maintain the ordered helical structures after the loading of TiO_2 nanocrystals. These highly dispersed crystals make the surface of CNT no longer smooth. Many TiO_2 nanoparticles are highly dispersed on the surface of CNT, and the rough surface is conducive to the SERS detection. To observe the distribution of TiO_2 inside the hollow structure of CNTs, the TEM and HRTEM of R-CNT/TiO_2 are shown in Figure 2. There is still a remarkable helical and hollow structure on CNT after the loading of TiO_2 (Figure 2 a), and the TiO_2 nanocrystals are indeed highly dispersed on the surface as well as inside the cavity of R-CNT (Figure 2 b). The HRTEM results indicate that many TiO_2 nanocrystals with circa 8 nm are authentically inside the hollow cavity of CNT (Figure 2 c), and the lattice spacing of $d \approx 0.352$ nm is ascribed to the (101) facet of anatase (Figure 2 d). Not surprisingly, the L-CNT/TiO_2 also has the similar TEM results with R-CNT/TiO_2 (Supporting Information, Figure S6).

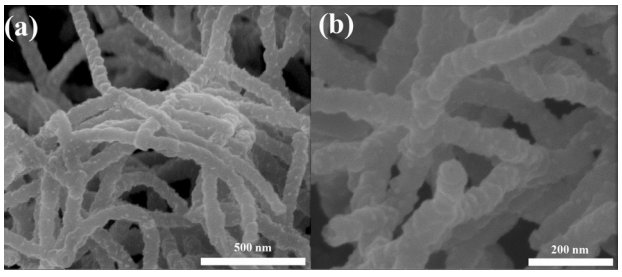

Figure 1. FESEM images of the R-CNT/TiO_2 hybrids. Scale bars: a) 500 nm, b) 200 nm.

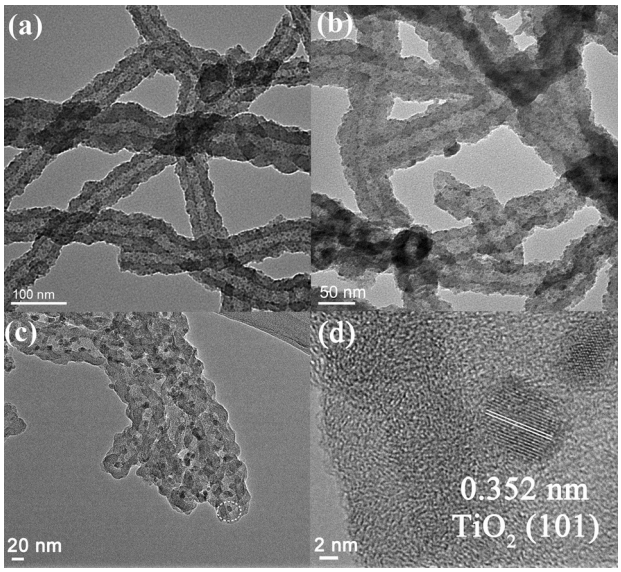

Figure 2. a,b) TEM and c,d) HRTEM images of the R-CNT/TiO_2 hybrids: d) amplification of the white dashed circle in (c).

In the process of SERS detection, the organic pollutant of MB (1×10^{-4} M) was used as the detected molecule, and various carbon-based nanotubes were employed as the substrate. The SEM images of the actual substrate used for the SERS measurement are shown in the Supporting Information, Figure S7. Compared with the blank glass substrate, the substrate coated with R-CNT/TiO_2 shows a distinct and uniform film covered on the surface of substrate. To eliminate the impact of the cavity effect and the adsorption effect of chiral CNTs on the SERS sensitivity, we chose the chirality-free commercial CNT (CCNT) having similar micromorphology and hollow structure with chiral CNT as the reference (TEM images in the Supporting Information, Figure S8 a). The TiO_2 nanocrystals are also highly dispersed on the surface of CCNT by the similar solvothermal method (Supporting Information, Figure S8 b,c). Raman spectra of MB adsorbed on the substrates coated with different CNTs in the absence of TiO_2 are shown in the Supporting Information, Figure S9. Compared to the CCNT without helical structure, all of the chiral CNTs including R- and L-CNT display a significant

Raman signal, indicating that the helical structure can help the improvement of the SERS sensitivity for the detection of MB, which does not result from the cavity effect and the adsorption of MB on CNT but from the birefringence induced by the helical structure (Scheme 1). Under laser irradiation, the chiral CNT easily undergoes the optical Kerr effect,[15] that is, the incident light will divide into two beams of refracted light along different directions (birefringence phenomenon); one is vertical the principal plane (along the normal) and another is inside the principal plane (Scheme 1). The presence of birefringence provides many more opportunities for the occurrence of Raman scattering, resulting in the improvement of SERS sensitivity of chiral CNTs for the detection of MB.

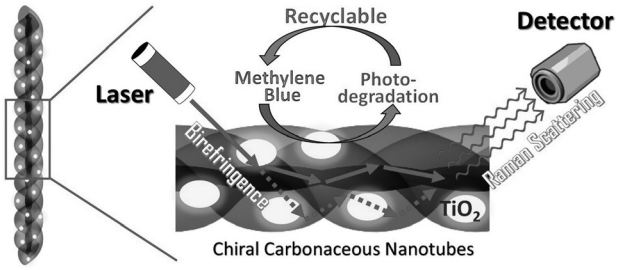

Scheme 1. Structural model of chiral CNT/TiO_2 and the plasmon-free and recyclable SERS detection of methylene blue over the chiral CNT/TiO_2 hybrids.

After the loading of TiO_2 nanocrystals, the L/R-CNT/TiO_2 hybrids still retain strong SERS signals for the detection of MB, and the intensity of SERS is almost unchanged (Figure 3a; Supporting Information, Figure S9, L-CNT: 11088.4 Cs^{-1} vs. L-CNT/TiO_2: 11009.9 Cs^{-1}). The detection limit of R-CNT and R-CNT/TiO_2 are all approximately 5×10^{-5} M (Supporting Information, Figure S10). In the case both with and without TiO_2, the L-CNTs exhibit a little higher enhancement of SERS than R-CNTs (Figure 3a; Supporting Information, Figure S9), which is mainly due to the difference in sample preparation. We have repeated the preparation of R-CNT and R-CNT/TiO_2 for the Raman detection, which gave a similar SERS intensity with the L-CNT based substrates (Supporting Information, Figure S11). Interestingly, both the L-CNT and R-CNT with a low concentration of MB (1×10^{-4} M) have a much stronger Raman signal intensity than that of the blank MB with a high concentration (1×10^{-2} M) (Supporting Information, Figure S12, 10588.4 Cs^{-1} vs. 10974.5 Cs^{-1} vs. 4828.0 Cs^{-1}), which further implies the presence of SERS enhancement over the helical structures. However, the reference of CCNT/TiO_2 only presents the characteristic D- and G-peaks of graphite of CNT (Figure 3a), indicating once again the important role of helical structure in the SERS sensitivity. For the recycling of substrate, we tried to put the substrates under the simulated solar light irradiation. Interestingly, no matter the R-CNT (Figure 3b) or the L-CNT (Supporting Information, Figure S13), their Raman signals have no any decrease after the irradiation of solar light for 20 min. Differently, after the loading of TiO_2, the Raman signals of L/R-CNT/TiO_2 have an obvious decrease after the irradiation (Figure 3c; Supporting Information, Figure S14a). After

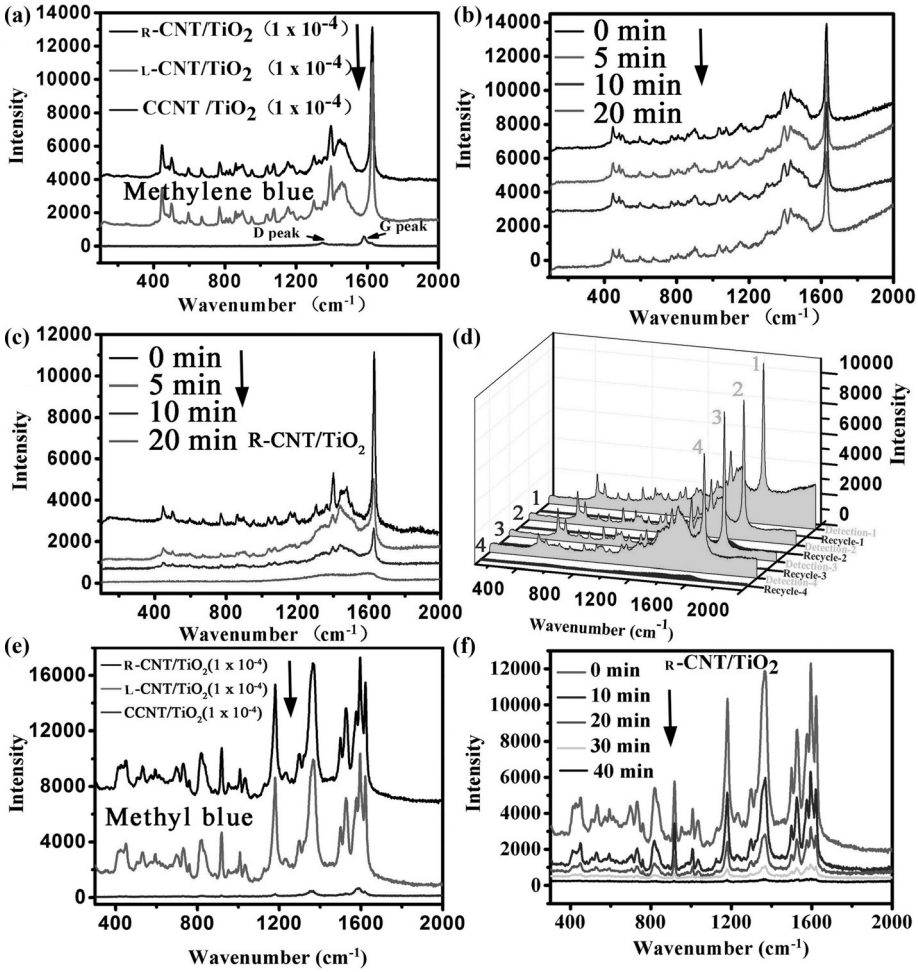

Figure 3. a) Comparison of Raman spectra of MB (1×10^{-4} M) adsorbed on R-CNT/TiO_2, L-CNT/TiO_2, and CCNT/TiO_2 (commercial CNT loaded with TiO_2). b,c) Raman spectra of 10^{-4} M MB adsorbed on blank R-CNT (b) and R-CNT/TiO_2 (c) under simulated solar light irradiation for different times (0–20 min). d) Recycling experiment test of R-CNT/TiO_2. The initial concentration of MB is 10^{-4} M, and the simulated solar light irradiation time is 20 min. e) Comparison between Raman spectra of methyl blue (1×10^{-4} M) adsorbed on R-CNT/TiO_2, L-CNT/TiO_2, and CCNT/TiO_2. f) Raman spectra of 10^{-4} M methyl blue adsorbed on R-CNT/TiO_2 under simulated solar light irradiation for different times (0–40 min).

irradiation for 20 min, the MB molecules absorbed on the L/R-CNT/TiO_2 have been photodegraded by the TiO_2 nanocrystals, which suggests the recyclable property of L/R-CNT/TiO_2 in the application of SERS detection. However, if the concentration of MB is much higher (10^{-2} M), it is really difficult to be completely degraded within the limited irradiation time (Supporting Information, Figure S14b), owing to the relative low percentage of TiO_2 (17.5 wt%) in the composite. Our next research will focus on how to improve the percentage of TiO_2 in the helical CNT/TiO_2 composites. Because of intrinsic self-cleaning ability of TiO_2, CNT/TiO_2 based substrate can decompose organic analyte (MB) under the solar light irradiation. The cyclic photodegradation of 10^{-4} M MB on R-CNT/TiO_2 was tested under simulated solar light irradiation, as shown in Figure 3d. After 4 cycles, the substrate coated with R-CNT/TiO_2 still shows excellent SERS activity, indicating the excellent stability and recyclability of chiral CNT/TiO_2 hybrids in the SERS detection, which is better than other self-cleaning substrate with recyclable plasmon-free SERS activity (easy decrease after the second cycle).[9] Along with MB, the methyl blue with different molecule structure and much more sulfonic groups was also used as the probe organic pollutant to demonstrate the popularity of chiral CNT/TiO_2 for the SERS detection (molecular structures are shown in the Supporting Information, Figure S15). Both L-CNT/TiO_2 and R-CNT/TiO_2 have a strong SERS signal compared with the commercial CCNT/TiO_2 (Figure 3e). After irradiation for 40 min, the methyl blue also can be photodegraded by the loaded TiO_2 nanocrystals (Figure 3f), indicating the SERS platform still be recyclable when used for the detection of other dye/compounds.

In fact, the absence of aggregation of TiO_2 nanoparticles favors the occurrence of birefringence for the SERS detection and the photodegradation of detected organic molecules (MB) for substrate recycling. For instance, the P25 was randomly loaded on the surface of R-CNT with a poor aggregation appearance (Figure 4a,b). The shielding of the helical structure by the P25 nanoparticles causes lower SERS signals compared with the R-CNT/TiO_2 (Figure 4c). Though the commercial P25 has an excellent photocatalytic activity, it is very difficult to detect the photodegradation of MB over the R-CNT/P25 by SERS owing to the heterogeneous dispersion of P25. Even after 20 min light irradiation, some weak SERS signals for MB can still be detected on the R-CNT/P25 (Figure 4d).

Very importantly, the enhancement factor (EF) of the R-CNT/TiO_2 substrate is evaluated to be about 3×10^3,[17] which is relatively good sensitivity for plasmon-free substrates for the application of SERS detection. Although many theoretical models have been used to explain the SERS effect, it is very difficult to clarify all the SERS phenomenon just by one model. Conventional SERS enhancement by plasmonic metallic nanoparticles has long been explained based on the two effects: electromagnetic and chemical. However, to the plasmon-free substrates, it is quite difficult to clearly explain the SERS by the above two models. Ling et al.[18] have demonstrated that some carbon materials such as graphene could also be used as a substrate for Raman enhancement.

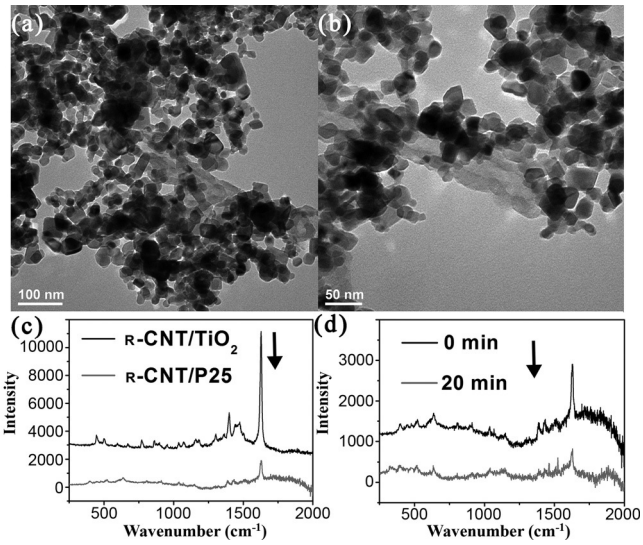

Figure 4. a,b) TEM images for the R-CNT loaded with P25 nanoparticles (R-CNT/P25). c) Comparison between Raman spectra of MB (1×10^{-4} M) adsorbed on R-CNT/TiO_2 and R-CNT/P25. d) Raman spectra of 10^{-4} M MB adsorbed on R-CNT/P25 under simulated solar light irradiation for 20 min.

They attributed the SERS enhancement to the charge transfer between graphene and the probe molecules, which resulted in a chemical effect for the enhancement of Raman signals. The graphene-induced SERS mainly relies on a chemical mechanism and therefore shows unique molecular selectivity. However, with an increase in the number of graphene layers, the Raman signals become weaker and weaker.[18b] The choice of molecular structures symmetry and substituents similar to that of the graphene structure are found to be favorable for SERS enhancement, which can be explained by group theory and the charge-transfer interactions between molecules and graphene. In our investigation, though the helical CNT has a similar structure of sp^2 C–C bonds to graphene, its electrical conductivity is much lower than that of graphene. On the other hand, compared with copper phthalocyanine (CuPc) and zinc phthalocyanine (ZnPc),[18b] the MB molecule does not have a D_{4h} symmetry structure, which cannot allow a strong interaction with CNT. Hence, the chemical effect of charge transfer between helical CNT and MB is not the major reason for the enhancement SERS sensitivity. Despite this, the chemical effect cannot be completely eliminated during the SERS detection over the CNT-based platform. The FTIR spectra of CCNT before and after adsorption of MB indicate that some chemical bonds are indeed generated between MB and CCNT (Supporting Information, Figure S16a). There is not an obvious difference of FTIR spectra between the R-CNT before and after MB adsorption (Supporting Information, Figure S16b), which is maybe owing to the overlap of the characteristic peaks of residual pyrrole rings in the range of 1000–1600 cm^{-1}.[2]

Generally, the chemical models emphasize the chemical adsorption between the molecules and substrates, and the SERS spectra should have an obvious difference from the conventional Raman spectra, such as a large frequency shift and the change of the relative intensities and positions of

characteristic peaks. However, here the SERS spectra of R-CNT adsorbed with MB is very similar with the conventional Raman spectra of blank MB (Supporting Information, Figure S12), indicating the significant SERS enhancement for the chiral CNT-based materials is mainly induced by the special helical structure rather than the traditional chemical effect. When the helical structure was shielded by the P25 nanoparticles, its SERS signals would be decreased distinct (Figure 4a–c), which indirectly demonstrate the importance of helical structure to its SERS enhancement. This result also indicates that the SERS enhancement effect is surface-sensitive and decays with analyte distance from the substrate surface.

In fact, the mechanism for the plasmon-free and recyclable SERS sensitivity of chiral CNT/TiO_2 is very simple and clear. As shown in Scheme 1, in the irradiation of laser, the generation of birefringence on the chiral CNT/TiO_2 leads to the multiple Raman scattering, which is responsible for the improved and plasmon-free SERS activity of MB. After the Raman detection, the surface-adsorbed MB molecules can be completely photodegraded by the highly dispersed TiO_2 nanocrystals under the solar light irradiation, which can realize the recycling of the chiral CNT/TiO_2 substrate.

To further demonstrate the importance of helical structure in the SERS detection, we choose three positions on different substrates at random from the Raman detection to record the MB signals (Supporting Information, Figure S17). There is not any enhanced SERS signal of MB on the commercial CCNT/TiO_2 platform at three random positions (Supporting Information, Figure S17a). However, there are obvious SERS signals over R-CNT/TiO_2 based substrate at all the random positions (Figure S17b). When the helical structure is shielded by the P25 nanoparticles, the SERS signal has a distinct reduction owing to the decrease of the light birefringence on the surface of R-CNT/P25 (Figure S17c). Compared with MB, the methyl blue molecule has many more hydrophilic sulfonic groups, which is beneficial to be chemically adsorbed on the surface of CNTs and induce the enhancement of Raman signals owing to the adsorption effect (Supporting Information, Figure S15). There is only a weak SERS signal of methyl blue at one position on the CCNT/TiO_2 platform among the four random positions (Supporting Information, Figure S18a), owing to the adsorption effect. However, strong SERS signals are observed at all four random positions over the R-CNT/TiO_2 platform (Supporting Information, Figure S18b). The above results indicate that the helical structure rather than the cavity effect or the adsorption effect of CNT is the main reason for the SERS sensitivity.

In conclusion, the chiral CNT was firstly and successfully used in the plasmon-free SERS detection, and the TiO_2 modification on the CNT realized the recycle of SERS substrate. The highly SERS-sensitive detection over the chiral CNT/TiO_2 hybrid was achieved by to the occurrence of birefringence induced by the unique helical structure. The highly dispersed TiO_2 nanocrystals on the surface and inside the cavity of CNTs can completely degrade the detected organic pollutants under solar light irradiation, which contributes to the recycle of the SERS substrate. The present investigation not only expands the application of chiral inorganic materials in the SERS, but also provides a new substrate materials used in the plasmon-free SERS detection.

Keywords: carbonaceous nanotubes · chiral structures · plasmon-free detection · surface-enhanced Raman scattering · titania

How to cite: *Angew. Chem. Int. Ed.* **2015**, *54*, 10643–10647
Angew. Chem. **2015**, *127*, 10789–10793

[1] S. Che, Z. Liu, T. Ohsuna, K. Sakamoto, O. Terasaki, T. Tatsumi, *Nature* **2004**, *429*, 281–284.
[2] S. Liu, Y. Duan, X. Feng, J. Yang, S. Che, *Angew. Chem. Int. Ed.* **2013**, *52*, 6858–6862; *Angew. Chem.* **2013**, *125*, 6996–7000.
[3] Y. Zheng, L. Lin, X. Ye, F. Guo, X. Wang, *Angew. Chem. Int. Ed.* **2014**, *53*, 11926–11930; *Angew. Chem.* **2014**, *126*, 12120–12124.
[4] S. Liu, L. Han, Y. Duan, S. Asahina, O. Terasaki, Y. Cao, B. Liu, L. Ma, J. Zhang, S. Che, *Nat. Commun.* **2012**, *3*, 1215.
[5] L. Ma, Y. Duan, Y. Cao, S. Asahina, Z. Liu, S. Che, *Chem. Commun.* **2013**, *49*, 11686–11688.
[6] B. F. G. Johnson, S. A. Raynor, D. S. Shephard, T. Mashmeyer, T. Mashmeyer, J. Meurig Thomas, G. Sankar, S. Bromley, R. Oldroyd, L. Gladden, M. D. Mantle, *Chem. Commun.* **1999**, 1167–1168.
[7] K. E. Shopsowitz, H. Qi, W. Y. Hamad, M. J. MacLachlan, *Nature* **2010**, *468*, 422–425.
[8] I. Hodgkinson, Q. h. Wu, *Adv. Mater.* **2001**, *13*, 889–897.
[9] D. Qi, L. Lu, L. Wang, J. Zhang, *J. Am. Chem. Soc.* **2014**, *136*, 9886–9889.
[10] a) C. S. Allen, R. P. Van Duyne, *J. Am. Chem. Soc.* **1981**, *103*, 7497–7501; b) J. Zhao, L. Jensen, J. Sung, S. Zou, G. C. Schatz, R. P. Van Duyne, *J. Am. Chem. Soc.* **2007**, *129*, 7647–7656.
[11] I. Alessandri, *J. Am. Chem. Soc.* **2013**, *135*, 5541–5544.
[12] I. Alessandri, L. E. Depero, *Chem. Commun.* **2009**, 2359–2361.
[13] I. Alessandri, M. Ferroni, L. E. Depero, *ChemPhysChem* **2009**, *10*, 1017–1022.
[14] C. Fan, H. Qiu, J. Ruan, O. Terasaki, Y. Yan, Z. Wei, S. Che, *Adv. Funct. Mater.* **2008**, *18*, 2699–2707.
[15] D. Wang, Y. Li, G. Li Puma, C. Wang, P. Wang, W. Zhang, Q. Wang, *Chem. Commun.* **2013**, *49*, 10367–10369.
[16] a) A. Fujishima, K. Honda, *Nature* **1972**, *238*, 37–38; b) R. Asahi, T. Morikawa, T. Ohwaki, K. Aoki, Y. Taga, *Science* **2001**, *293*, 269–271; c) J. Schneider, M. Matsuoka, M. Takeuchi, J. Zhang, Y. Horiuchi, M. Anpo, D. W. Bahnemann, *Chem. Rev.* **2014**, *114*, 9919–9986; d) B. Qiu, M. Xing, J. Zhang, *J. Am. Chem. Soc.* **2014**, *136*, 5852–5855; e) J. R. Swierk, N. S. McCool, T. P. Saunders, G. D. Barber, T. E. Mallouk, *J. Am. Chem. Soc.* **2014**, *136*, 10974–10982; f) A. S. Hall, A. Kondo, K. Maeda, T. E. Mallouk, *J. Am. Chem. Soc.* **2013**, *135*, 16276–16279.
[17] a) S. Lal, N. K. Grady, G. P. Goodrich, N. J. Halas, *Nano Lett.* **2006**, *6*, 2338–2343; b) A. D. McFarland, M. A. Young, J. A. Dieringer, R. P. Van Duyne, *J. Phys. Chem. B* **2005**, *109*, 11279–11285; c) E. C. Le Ru, E. Blackie, M. Meyer, P. G. Etchegoin, *J. Phys. Chem. C* **2007**, *111*, 13794–13803; d) Y. Hu, Y. Shi, H. Jiang, G. Huang, C. Li, *ACS Appl. Mater. Interfaces* **2013**, *5*, 10643–10649.
[18] a) X. Ling, L. Xie, Y. Fang, H. Xu, H. Zhang, J. Kong, M. S. Dresselhaus, J. Zhang, Z. Liu, *Nano Lett.* **2010**, *10*, 553–561; b) S. Huang, X. Ling, L. Liang, Y. Song, W. Fang, J. Zhang, J. Kong, V. Meunier, M. S. Dresselhaus, *Nano Lett.* **2015**, *15*, 2892–2901.

Received: June 10, 2015
Published online: July 14, 2015

